Acta Biochim Biophys Sin 2022, 54(12): 1874–1888
https://doi.org/10.3724/abbs.2022175
Advance Access Publication Date: 14 December 2022
Original Article

Original Article

miR-96-5p regulates myocardial infarction-induced cardiac fibrosis via Smad7/Smad3 pathway

Huanyu Gu[1], Yi Duan[2], Shanshan Li[1], Qin Wang[1], Wen Zhen[1], Wei Zhang[1], Yingying Zhang[3], Min Jiang[1,*], and Chun Wang[1,*]

[1]Department of Geriatrics, Nanjing Drum Tower Hospital, the Affiliated Hospital of Nanjing University Medical School, Nanjing 210008, China, [2]Department of Ophthalmology, Shanghai General Hospital, Shanghai Jiao Tong University, Shanghai 200080, China, and [3]School of Basic Medicine and Clinical Pharmacy, China Pharmaceutical University, Nanjing 210009, China
*Correspondence address. Tel: +86-25-83106666; E-mail: wangchun@njglyy.com (C.W.) / E-mail: jmin1212@hotmail.com (M.J.)

Received 14 July 2022 Accepted 27 August 2022

Abstract

Fibrotic remodelling contributes to heart failure in myocardial infarction. MicroRNAs (miRNAs) play a crucial role in myocardial fibrosis. However, current antifibrotic therapeutic strategies using miRNAs are far from effective. In this study, we aim to investigate the effect of miR-96-5p on cardiac fibrosis. Our work reveals a significant upregulation of miR-96-5p level in the ventricular tissues of myocardial infarction mice, as well as in neonatal rat cardiac fibroblasts stimulated with TGF-β or Ang II as shown by qPCR assay. In myocardial infarction mice, *miR-96-5p* knockdown using antagomir alleviates the aggravated cardiac fibrosis and exacerbated myocardial function caused by myocardial infarction surgery as shown by the echocardiography and Masson's staining analysis. In contrast, immunofluorescence staining results reveal that miR-96-5p overexpression in neonatal rat cardiac fibroblasts contributes to an increase in the expressions of fibrosis-associated genes and promotes the proliferation and differentiation of cardiac fibroblasts. Conversely, miR-96-5p downregulation using inhibitor presents adverse consequences. Furthermore, Smad7 expression is downregulated in fibrotic cardiac tissues, and the *Smad7* gene is identified as a direct target of miR-96-5p by dual luciferase assay. Indeed, *Smad7* knockdown weakens the antifibrotic effect of the miR-96-5p inhibitor on cardiac fibroblasts. Moreover, Smad3 phosphorylation is elevated in fibrotic cardiac tissues, and interestingly, the Smad3 inhibitor suppresses the profibrotic effect of the miR-96-5p mimic. Taken together, our findings demonstrate that the Smad7/Smad3 signaling pathway mediates the profibrotic effect of miR-96-5p in cardiac fibrosis.

Key words myocardial infarction, cardiac fibrosis, miR-96-5p, Smad7, Smad3

Introduction

As one of the most prevalent cardiovascular diseases, myocardial infarction (MI) leads to severe morbidity and mortality worldwide [1]. This multigene disease is characterized by chronic complicated fibrotic remodelling and cardiomyocyte hypertrophy [2]. Cardiac fibrosis participates in ventricle remodelling by preserving the structural and functional integrity of injured ventricles at the initial stage and progressively causing cardiac contractile dysfunction at later stages, resulting in lethal arrhythmia and heart failure [3,4]. Effective therapies for cardiac fibrosis can ameliorate cardiac function and improve the prognosis of MI. Nevertheless, valid and clinically safe treatment modalities are lacking [5]. Hence, developing novel functional therapeutic targets is essential to facilitate the clinical intervention of cardiac fibrosis.

Understanding the cardiac fibrotic process and its underlying mechanisms is pivotal for identifying novel anti-fibrotic regulators. The progression of cardiac fibrosis is determined by three distinguishing features: the proliferation of cardiac fibroblasts (CFs), fibroblast-to-myofibroblast transition (FMT), and excessive extracellular matrix (ECM) deposition [6]. CFs are the main cells responsible for cardiac fibrosis; they transform into myofibroblasts under environmental stimuli or pathologic stresses, disrupting homeostasis between fibrillar collagen degradation and synthesis [7]. Myocardial interstitial collagen deposition perturbs the ven-

tricular architecture and cardiac function as a consequence [8]. There are various molecular mechanisms underlying myocardial fibrosis, including the renin/angiotensin/aldosterone system, numerous inflammatory cytokines, transforming growth factor β (TGF-β), and platelet-derived growth factor [9]. The TGF-β/SMAD and Wnt pathways also strongly contribute to myocardial fibrosis [10,11].

It is well established that microRNAs (miRNAs) are implicated in mediating cardiac fibrosis. miRNAs are small noncoding single-stranded RNAs that specifically recognize and bind with the 3′-UTR of target mRNAs, leading to posttranscriptional degradation of downstream genes [12]. miRNAs regulate nearly 60% of protein-coding genes involved in multiple biological processes, such as differentiation, proliferation, aging, and apoptosis [13]. Several studies have verified that miRNAs are intimately associated with cardiac fibrosis. For example, miR-214-3p and miR-451a exert anti-fibrotic properties, while miR-21 and miR-99-3p exhibit pro-fibrotic effects [14–17].

An unexplored candidate, miR-96-5p, which was previously focused in the field of tumor development [18,19], has been recently explored in fibrosis-associated studies. For example, it can promote the differentiation of orbital fibroblasts [20]. Moreover, it is upregulated in viral hepatitis B-induced hepatic fibrosis [21]. Another study reported that the miR-96-5p level was enhanced in human fibrotic liver tissues and suppressed profibrogenic activation of hepatic stellate cells [22]. For renal fibrosis, miR-96-5p exerted an antifibrotic effect on diabetic kidney disease [23]. Meanwhile, miR-96-5p lowered hypoxia-induced apoptosis in cardiomyocytes [24]. Nonetheless, the precise function of miR-96-5p in cardiac fibrosis remains unknown and hence warrants further investigation.

The TGF-β pathway possesses multifunctional roles in organ fibrosis and other essential biological regulatory mechanisms, in which Smad3 is a confirmed major downstream molecule [25,26]. In injuries, secretion of TGF-β1 and activation of the Smad pathway are two main inducers of FMT and ECM synthesis [27]. In addition to TGF-β1, Smad3 can also be activated by angiotensin II (Ang II), a critical mediator of the renin–angiotensin system and contributor to hypertension [28]. In the TGF-β/Smad signal transduction pathway, Smad7 acts as a negative regulator that can inhibit cardiac fibrosis by blocking the phosphorylation and activation of Smad3 or Smad2 [29]. MiR-192 and miR-217 have been identified as key mediators of cardiac fibrosis triggered by TGF-β and Smad3 phosphorylation [30]. Previous research demonstrated that miR-21 promoted cardiac fibrosis by targeting Smad7 [31]. However, whether miR-96-5p affects myocardial fibrosis through TGF-β/Smad pathway is unknown.

In the present study, we investigated the effect of miR-96-5p on cardiac fibrosis. We found that miR-96-5p was upregulated both in the cardiac infarct zone after MI and fibrotic neonatal rat cardiac fibroblasts (NRCFs). MI-induced cardiac fibrosis and dysfunction were attenuated by systemic delivery of miR-96-5p antagomir. The miR-96-5p mimic enhanced the expression levels of fibrosis-associated genes in NRCFs and accelerated their proliferation and differentiation. Furthermore, Smad7 was validated as a direct target gene of miR-96-5p; it affected cardiac fibrosis through downstream Smad3 signaling. Collectively, our results support the profibrotic effect of miR-96-5p on myocardial fibrosis, providing a potential therapeutic target for the treatment of cardiac fibrosis following MI.

Materials and Methods

Ethics statement

Animals were handled according to the Guide for the Care and Use of Laboratory Animals published by the US National Institutes of Health (NIH, 8th Edition, National Research Council, 2011). Experimental protocols for animals were approved by the Animal Ethical Committee of Nanjing Drum Tower Hospital (Approval No. 2021AE01061).

Isolation, culture, and treatment of cells

Neonatal SD rats (1–3 days old) were obtained from Hangzhou Medical College (Hangzhou, China). The cardiac tissues of neonatal rats were digested with 0.25% trypsin (Beyotime, Shanghai, China). The cell pellets were cultured in 10-cm dishes in DMEM (Keygen, Nanjing, China) supplemented with 10% fetal bovine serum (FBS; Gibco, Grand Island, USA) and 1% streptomycin/penicillin. After 2 h, the cell cultures were subject to gravity separation: the supernatant was collected and centrifuged (800 *g*, 5 min) to acquire the neonatal rat cardiac myocytes (NRCMs); and the attached cells were NRCFs. Both NRCFs and NRCMs were maintained in DMEM containing 10% FBS, 1% streptomycin/penicillin in 5% CO_2 at 37°C. For the construction of two cell fibrosis models, second-passage NRCFs were stimulated using TGF-β1 (20 ng/mL; Peprotech, Rocky Hill, USA) or Ang II (200 nM; Sigma, St Louis, USA) for 48 h.

Transfections of the NC mimic (miR01101, 100 nM; RiboBio, Guanzhou, China) or miR-96-5p mimic (miR10000818, 100 nM; RiboBio), NC inhibitor (miR02101, 200nM; RiboBio) or miR-96-5p inhibitor (miR20000818, 200 nM; RiboBio), NC siRNA (forward: 5′-UUCUCCGAACGUGUCACGUTT-3′ and reverse: 5′-ACGUGACACGUUCGGAGAATT-3′, 50 nM; Sangon, Shanghai, China) or Smad7 siRNA (forward 5′-CTCCAGATACCCGATGGATTT-3′ and reverse 5′-AAATCCATCGGGTATCTGGAG-3′, 50 nM; Sangon) were performed in growth medium (DMEM + 1% FBS) using Lipofectamine 2000 (Invitrogen, Carlsbad, USA) according to the manufacturer's instructions. The Smad3 inhibitor SIS3 (1 μM; Sigma) was used to treat NRCFs for 48 h in the presence of miR-96-5p mimic.

Quantitative real-time polymerase chain reaction (qPCR)

TRIzol reagent (Invitrogen) was used to extract total RNA from the cells or left ventricles. The RNA concentration was measured with a NanoPhotometer (IMPLEN, Munich, Germany). RNA was reversely transcribed into cDNA using 400 ng of purified RNA with the PrimeScript RT reagent kit (Takara, Tokyo, Japan). qPCR was performed on a QuantStudio Real-Time PCR Instrument (Thermo Fisher, Waltham, USA). The Bio-Rad SYBR qPCR kit (Bio-Rad, Hercules, USA) was employed to detect mRNA levels, and the Bulge-Loop™ miRNA qPCR Primer Set (Ribobio) was used to detect miRNA levels. qPCR was performed under the following condition: denaturation at 95°C for 10 min, followed by 40 cycles at 95°C for 15 s and 60°C for 1 min. $2^{-\Delta\Delta Ct}$ method was used to calculate the relative values of mRNA and miRNA [32]. mRNA expression was normalized to 18S RNA, while expression of miRNA was normalized to 5S RNA. Primer sequences are listed in Table 1.

Immunofluorescence staining and EdU assay

NRCFs were fixed in 4% formaldehyde for 20 min, followed by permeabilization with 0.2% Triton X-100 for 15 min. The monolayers were then incubated with α-SMA-Cy3 (1:200; Sigma) for 2 h. Afterward, an EdU assay was performed using the kFluor488 Click-

Table 1. Sequences of primers used in this study for qPCR

Gene	Species	Forward primer (5′→3′)	Reverse primer (5′→3′)
α-SMA	Mouse	GTCCCAGACATCAGGGAGTAA	TCGGATACTTCAGCGTCAGGA
	Rat	GTCCCAGACATCAGGGAGTAA	TCGGATACTTCAGCGTCAGGA
Col1a1	Mouse	TCTAGACATGTTCAGCTTTGTGGAC	TCTGTACGCAGGTGATTGGTG
	Rat	GAGCGGAGAGTACTGGATCGA	CTGACCTGTCTCCATGTTGCA
Col3a1	Mouse	CTGTAACATGGAAACTGGGGAAA	CCATAGCTGAACTGAAAACCACC
	Rat	TGCCATTGCTGGAGTTGGA	GAAGACATGATCTCCTCAGTGTTGA
18s	Mouse	TCAAGAACGAAAGTCGGAGG	GGACATCTAAGGGCATCAC
	Rat	TCAAGAACGAAAGTCGGAGG	GGACATCTAAGGGCATCAC
BNP	Rat	GCTGCTGGAGCTGATAAGAGAA	GTTCTTTTGTAGGGCCTTGGTC
Smad7	Rat	CCGTGCAGATTAGCTTCGT	TCCTCTTCTCCCCACACC

iT EdU kit (Keygen) according to the standard procedure. Cell nuclei were stained with DAPI. Fluorescence was visualized under a fluorescence microscope (Thunder Imager; Leica Microsystem, Wetzlar, Germany). The numbers of EdU^+ cells and $DAPI^+$ cells and the fluorescence intensity of α-SMA were measured by ImageJ software (NIH, Bethesda, USA).

Western blot analysis

NRCFs or left ventricular tissues were homogenized in lysis buffer containing PMSF (Keygen). To obtain proteins of high purity, lysates were centrifuged at 12,000 *g* for 15 min. The bicinchoninic acid protein assay kit (Thermo Fisher) was used to measure the protein concentration. Each sample containing 20 μg of protein was separated by 10% SDS-PAGE (Bio-Rad) and then transferred onto a PVDF membrane (Millipore, Billerica, USA). Thereafter, the proteins were probed with primary antibodies against α-SMA (1:1000; Abclonal, Wuhan, China), CTGF (1:500; Abclonal), Col1a1 (1:1000; Abclonal), Col3a1 (1:1000; Abclonal), Smad7 (1:500; Abclonal), Smad3 (1:500; Abclonal), phospho-Smad3 (1:500; Abclonal), and GAPDH (1:2000; Abclonal). Subsequently, the membranes were incubated with a secondary antibody, namely, HRP-linked goat anti-rabbit IgG (1:5000; Abclonal). Finally, the signals were detected using an ECL kit (Tanon, Shanghai, China) on an imaging system (Tanon), and the blots were quantified with ImageJ software.

miRNA target prediction

miRDB (http://mirdb.org/), TargetScan (http://www.targetscan.org), and miRecords (http://c1.accurascience.com/miRecords/) were applied to predict potential targets of miR-96-5p. In total, 144 miRNAs overlapped on these three websites.

Dual luciferase assay

PCR amplification was performed to acquire the 3′UTR fragment of *Smad7* containing the target site of miR-96-5p. The PCR products were cloned into the pmirGLO Dual Luciferase vector (Promega, Madison, USA) to obtain the Smad7 vector. After 48 h of transfection, 293T cells were harvested, and luciferase activity was determined with a Dual-luciferase Reporter Assay System (Promega) according to the manufacturer's instructions. Firefly luciferase activity was normalized to Renilla luciferase activity.

Animal study

All animals were maintained in the Laboratory Animal Center of Nanjing Drum Tower Hospital (Nanjing, China), where the temperature (22°C), light (12 h light-dark cycle), and humidity are well controlled. Eight-week-old male C57BL/6 mice weighing 25 g (Hangzhou Medical College, Hangzhou, China) were subject to sham or MI surgery. Prior to surgery, the mice were injected with NC antagomir (miR3N0000003; RiboBio) or miR-96-5p antagomir (miR30000541; RiboBio) at 80 mg/kg via the tail vein for 3 consecutive days. During MI surgery, mice were intubated after anesthesia, and then the fourth ribs were cut. Then, a 7-0 silk suture was used to ligate the left anterior descending artery. Finally, a 6-0 silk suture was used to close the skin. Mice in the sham group were also subjected to the aforementioned procedure, but the arteries were not ligated. Then, 6 mice were used for miRNA sequencing, of which 3 mice underwent sham operation and the remaining mice underwent MI surgery. Another 20 mice were divided into 4 groups (sham + NC antagomir, sham + miR-96-5p antagomir, MI + NC antagomir, and MI + miR-96-5p antagomir), with 5 mice in each group. All mice were sacrificed for subsequent experiments 3 weeks post-MI after an echocardiographic assessment.

Echocardiographic study

Three weeks after the surgery, ventricular function was evaluated with an ultrasound Vevo 3100 system (VisualSonics Inc, Toronto, Canada) equipped with a 30 MHz phased array ultrasonic probe. Cardiac function was assessed by measuring fractional shortening (FS), ejection fraction (EF), left ventricle internal diameter during systole (LVIDs) and left ventricle internal diameter during diastole (LVIDd) with Vevo 3100 system from the cardiac long axis at the papillary muscle level.

MiRNA sequencing (miR-Seq) and identification of differentially expressed genes

RNA was extracted from 50 mg ventricular tissue using the Universal RNA Extraction Mini Kit (Aowei Biotech Co., Ltd, Foshan, China). Libraries for sRNA sequencing were prepared using the VAHTS Small RNA Library Prep Kit for Illumina (Vazyme, Nanjing, China) by Xu Ran Biotechnology Co., Ltd (Shanghai, China). In addition, 1 μg of total RNA was used as the input for RNA adapter ligation (using 3′ and 5′ RNA adapters) prior to reverse transcription and PCR amplification with bar-coded primers. Magnetic beads were used to recover the fractions containing mature miRNAs from the PCR products. The resulting small RNA libraries were concentrated by ethanol precipitation and quantified using a Qubit 2.0 Fluorometer (Thermo Fisher) prior to sequencing on a

NovaSeq6000 sequencer (Illumina, San Diego, USA) with read lengths of 50 base pairs and 15 million single-end reads per sample, on average.

Raw reads were first filtered based on stringent read quality control and then aligned and mapped to the Ensembl GRCh38 human reference genome using Bowtie. Mapped reads were subsequently annotated using genome annotation data from miRBase. The sum of all isomiR reads from the canonical mature miRNA locus was used for miRNA expression analysis. Differentially expressed miRNAs were identified using the DESeq software 1.34.1.

Masson's collagen staining

Myocardial specimens were fixed in 4% paraformaldehyde and then dehydrated using gradient ethanol. Tissues were sliced into 5-μm sections after being embedded in paraffin, and Masson staining was performed using Masson kit (Keygen) according to the manufacturer's protocol. Images of the stained slices were captured with an optical microscope (BX43; Olympus, Tokyo, Japan). The collagen volume fraction was determined by calculating the collagen area/total area using ImageJ software.

Statistical analysis

Data were analysed using Prism 6 (GraphPad Software, San Diego, USA) and SPSS 18.0 (IBM, Armonk, USA). The results are presented as the mean ± SD of 3, 5 or 6 duplicates. Student's *t*-test was used to compare differences between the two groups. One-way ANOVA was employed to compare differences among three or four groups. $P < 0.05$ was considered statistically significant.

Results

miR-96-5p expression is elevated in cardiac fibrosis

Total RNA was extracted from ventricular tissues of sham and MI mice for miR-seq to determine the miRNAs responsible for cardiac fibrosis after MI (Figure 1A and Supplementary Table S1). A series of miRNAs were dysregulated in the MI group, among which miR-96-5p expression was significantly upregulated. miR-96-5p has previously been studied in orbital fibroblast differentiation and in liver and kidney fibrosis [20–23]. These previous conclusions made our experiments more evidence-based. However, miR-96-5p has not been associated with cardiac fibrosis so far. The other miRNAs listed in Supplementary Table S1 with higher fold change than miR-96-5p, such as miR-382-5p, miR-411-5p, miR-370-3p, and miR-31-5p, as well as their relationships with fibrosis in any other organ have never been studied. miR-199a-5p and miR-136-5p were shown to promote cardiac fibrosis [33,34], while miR-455-3p was proven to inhibit the process of myocardial fibrosis [35]. Thus, the role of miR-96-5p in cardiac fibrosis was assessed in this study.

The qPCR array validated that the miR-96-5p level was markedly elevated in the infarct zone of the heart and this upregulation was accompanied by an increase in alpha-smooth muscle actin (α-SMA) expression, which is a sensitive indicator of fibrosis (Figure 1B,C). Additionally, miR-96-5p expression was evidently upregulated in the two different cardiac fibrosis models of TGF-β- or Ang-II-treated NRCFs (Figure 1D,E). In addition to cardiac fibroblasts, cardiomyocytes are another major cell type in the heart. Our results revealed that miR-96-5p was more enriched in NRCFs than in NRCMs (Figure 1F). Collagen type I alpha 1 (Col1a1) and Col3a1 are predominant cardiac collagens, while brain natriuretic peptide (BNP) is a marker of pathological hypertrophy. However, we found that their levels were unaffected by miR-96-5p in NRCMs (Figure 1G,H). Given that increased miR-96-5p expression might be related to cardiac fibrosis, its role was explored in cardiac fibroblasts but not in cardiomyocytes.

Inhibition of miR-96-5p ameliorates cardiac fibrosis after MI in mice

To investigate whether miR-96-5p is responsible for MI-induced fibrotic remodelling *in vivo*, a mouse model of MI-induced cardiac fibrosis was established after administration of NC antagomir or miR-96-5p antagomir into different groups of mice via tail vein injection. Hence, four groups were established: sham + NC antagomir, sham + miR-96-5p antagomir, MI + NC antagomir, and MI + miR-96-5p antagomir. qPCR results revealed that miR-96-5p expression was effectively knocked down by the miR-96-5p antagomir (Figure 2A). In subsequent research, the degree of cardiac fibrosis and cardiac function was not significantly altered under normal conditions. Echocardiography revealed that EF and FS were markedly decreased, whereas LVIDs and LVIDd were elevated in MI hearts. Meanwhile, miR-96-5p deficiency attenuated the impaired cardiac structure and function following MI (Figure 2B). Next, the degree of myocardial fibrosis was assessed by Masson's staining. The results showed that miR-96-5p inhibition reduced the fibrotic areas in MI heart tissue sections (Figure 2C). Consistently, the mRNA and protein levels of Col1a1, Col3a1, and α-SMA in the MI + miR-96-5p antagomir group were lower than those in the MI + NC antagomir group, as was the protein level of connective tissue growth factor (CTGF) (Figure 2D,E). These results implicated the role of miR-96-5p in cardiac fibrosis induced by MI.

miR-96-5p regulates the proliferation and differentiation of cardiac fibroblasts *in vitro*

In a subsequent experiment, the function of miR-96-5p in cardiac fibrosis with NRCFs was explored. First, the miR-96-5p mimic and inhibitor effectively regulated miR-96-5p expression in NRCFs (Figures 3A and 5A). miR-96-5p overexpression enhanced the mRNA levels of Col1a1, Col3a1, and α-SMA under basal conditions. Increases in the mRNA expressions of fibrosis-related genes were observed in TGF-β-treated NRCFs. However, miR-96-5p overexpression failed to further increase the mRNA levels of these genes in TGF-β-stimulated NRCFs (Figure 3B). Immunofluorescence staining was utilized to assess proliferation and differentiation abilities. The proliferation of NRCFs was determined by calculating the EdU^+ cell number/$DAPI^+$ cell number, and the differentiation of NRCFs was indicated by the fluorescence intensity of α-SMA. As expected, the miR-96-5p mimic improved both abilities of NRCFs at the basal level in the absence of TGF-β (Figure 3C). Consistent with the above results, the miR-96-5p mimic elevated the protein levels of Col1a1 and α-SMA in NRCFs (Figure 3D). Similar results were obtained in the cell model of myocardial fibrosis stimulated with Ang II, corroborating the effect of the miR-96-5p mimic in NRCFs (Figure 4). In contrast, the miR-96-5p inhibitor had the opposite effects both under basal conditions and after treatment with TGF-β or Ang II (Figures 5 and 6). Taken together, these results confirmed that miR-96-5p facilitates cardiac fibrosis *in vitro*.

Smad7 is a direct target of miR-96-5p

To elucidate the underlying molecular mechanisms, three databases

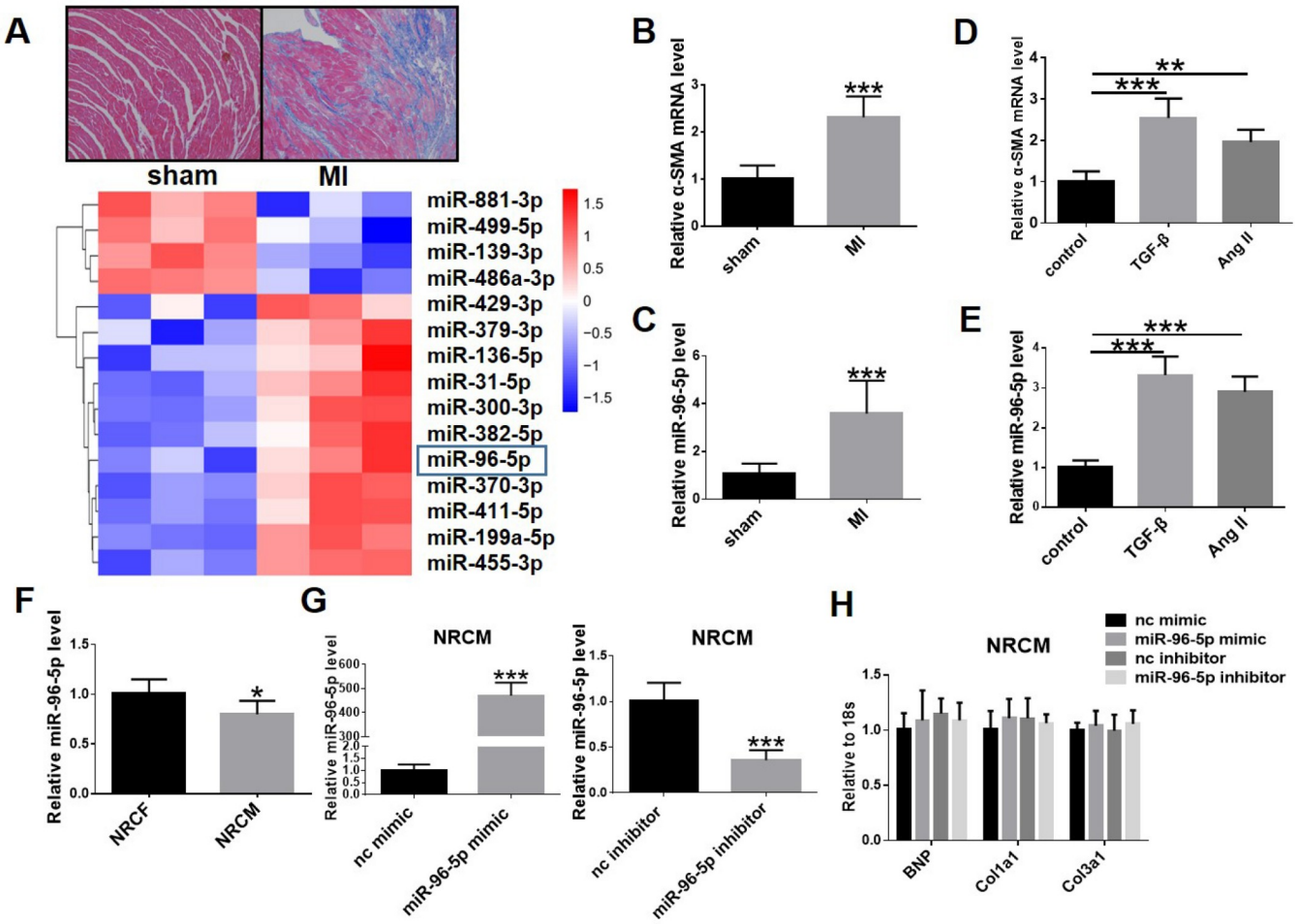

Figure 1. Increased miR-96-5p is associated with cardiac fibrosis (A) miR-seq analysis of cardiac samples from mice undergoing sham and MI surgeries ($n=3$). (B) The relative mRNA level of α-SMA ($n=5$). (C) qPCR analysis of miR-96-5p expression ($n=5$). (D,E) The relative α-SMA mRNA and miR-96-5p expression levels of two *in vitro* cardiac fibrosis models (NRCFs stimulated with 20 ng/mL TGF-β or 200 nM Ang II for 48 h, $n=5$). (F) miR-96-5p levels in NRCFs versus NRCMs ($n=5$). (G) Expression of miR-96-5p in NRCMs transfected with miR-96-5p mimic or inhibitor ($n=5$). (H) The relative mRNA levels of BNP, Col1a1, and Col3a1 in NRCMs transfected with miR-96-5p mimic or inhibitor ($n=5$). $^{*}P<0.05$, $^{**}P<0.01$, $^{***}P<0.001$ vs corresponding controls.

(TargetScan, miRDB, and miRecords) were used to search for potential fibrosis-associated targets of miR-96-5p (Figure 7A). Finally, 144 potential candidates were identified, among which Smad7 was verified to have an established role in regulating cardiac fibrosis [29]. The databases revealed conserved binding sites between miR-96-5p and *Smad7*. Next, dual-luciferase reporter assay showed that wild-type (WT) Smad7 was repressed by miR-96-5p, whereas mutant Smad7 was not (Figure 7B). As miRNAs regulate target genes at the posttranscriptional level, western blot analysis was performed and the results revealed that the protein level of Smad7 was negatively regulated by miR-96-5p (Figure 7C). These data demonstrate that *Smad7* is a direct target gene of miR-96-5p.

Additionally, we examined whether Smad7 mediates the effect of miR-96-5p on myocardial fibrosis. Contrary to the miR-96-5p variation tendency, the protein level of Smad7 was lower in NRCFs exposed to TGF-β or Ang II than in the control (Figure 7D). The Smad7 siRNA used in the following experiments effectively silenced the expression of Smad7 (Figure 7E). Functional rescue experiments confirmed that *Smad7* knockdown weakened the anti-fibrotic effect of the miR-96-5p inhibitor (Figure 8). Altogether, these data strongly supported the hypothesis that *Smad7* is a direct target gene mediating the effect of miR-96-5p in cardiac fibrosis.

miR-96-5p promotes cardiac fibrosis by regulating the Smad7/Smad3 signaling pathway

Since Smad7 was proven to limit fibrosis progression by blocking TGF-β1/Smad signaling pathway, we further explored whether miR-96-5p promotes cardiac fibrosis by modulating Smad7 and its downstream effector Smad3, which is vital for the activation of cardiac fibroblasts [29]. Western blot analysis revealed that *Smad7* knockdown activated Smad3 phosphorylation (Figure 9A). Smad7 expression was decreased, whereas the phosphorylation level of Smad3 was elevated in fibrotic heart tissue, compared with those in the sham group (Figure 9B). In addition, the Smad3 inhibitor downregulated the levels of Col1a1, Col3a1, and α-SMA, thereby reducing the proliferation and differentiation of NRCFs. Interestingly, the Smad3 inhibitor blocked the profibrotic effect of the miR-96-5p mimic (Figure 9C–E). These results indicated a potential correlation between miR-96-5p and Smad7/Smad3 signaling in

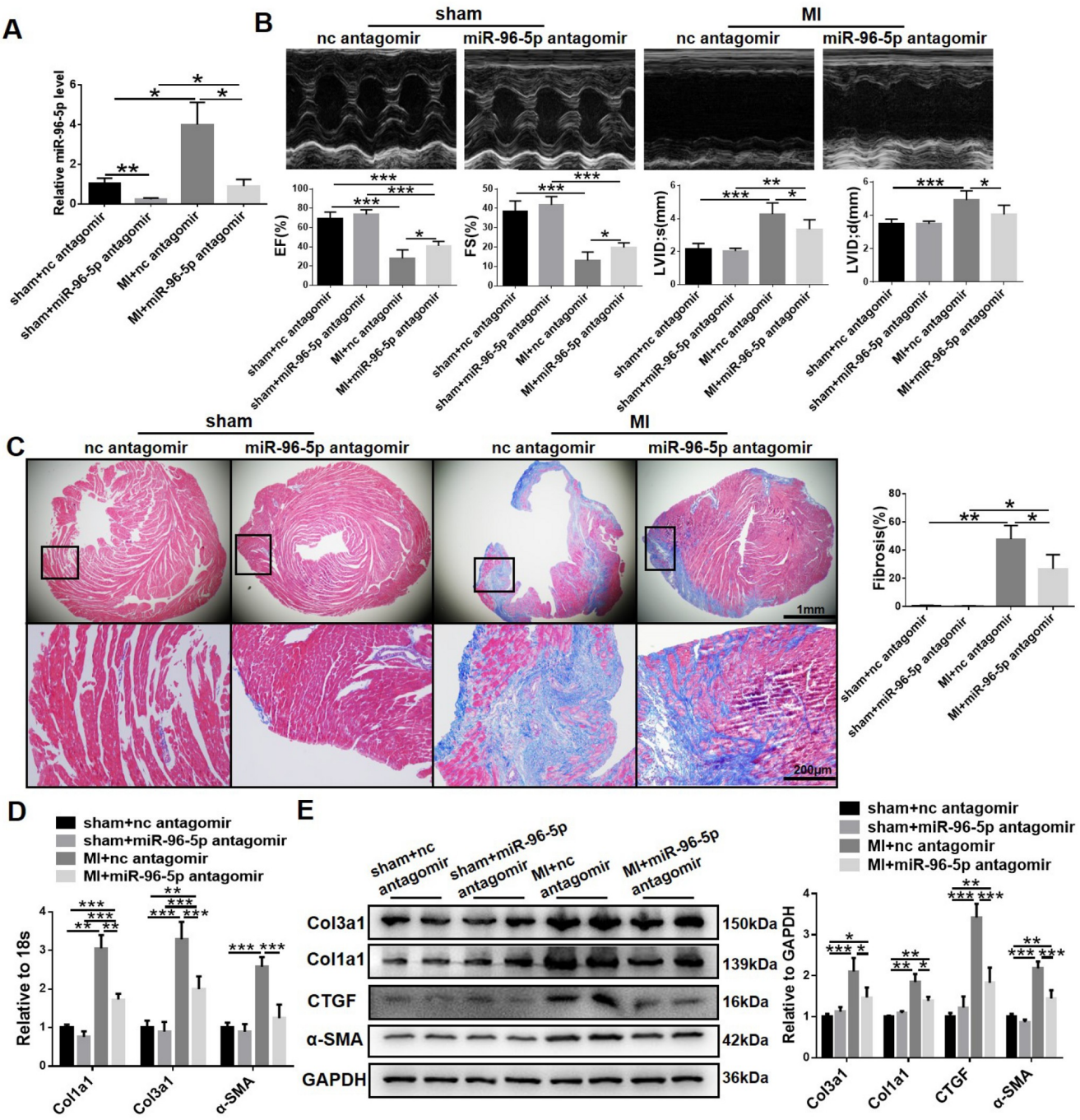

Figure 2. Inhibition of miR-96-5p alleviates myocardial fibrosis in post-MI mice (A) qPCR analysis of miR-96-5p expression in the heart chamber ($n=5$). (B) Mouse cardiac function was measured by EF%, FS%, LVIDs, and LVIDd ($n=5$). (C) Images and measurement of Masson's trichrome-stained cardiac sections ($n=5$). Upper scale bar: 1 mm; lower scale bar: 200 μm. (D) The relative mRNA levels of Col1a1, Col3a1, and α-SMA in ventricular tissues ($n=5$). (E) Protein levels of Col1a1, Col3a1, CTGF, and α-SMA in ventricular tissues determined by western blot analysis ($n=5$). $^{*}P<0.05$, $^{**}P<0.01$, $^{***}P<0.001$ vs corresponding controls.

regulating cardiac fibrosis.

Discussion

The current study illustrated the relationship between miR-96-5p and cardiac fibrosis both *in vitro* and *in vivo*. First, the MI mouse model was constructed. Based on the analysis of miR-seq and qPCR, miR-96-5p was enhanced in post-MI cardiac fibrosis. Inhibiting miR-96-5p by antagomir preserved ventricular function and attenuated cardiac fibrosis induced by MI. Second, at the cellular level, TGF-β- or Ang II-treated NRCFs were used to construct cell models. Gain- and loss-of-function experiments revealed that overexpression of miR-96-5p accelerated cardiac fibroblast proliferation and differentiation to myofibroblasts, whereas miR-96-5p inhibition reversed these effects. Third, dual luciferase reporter

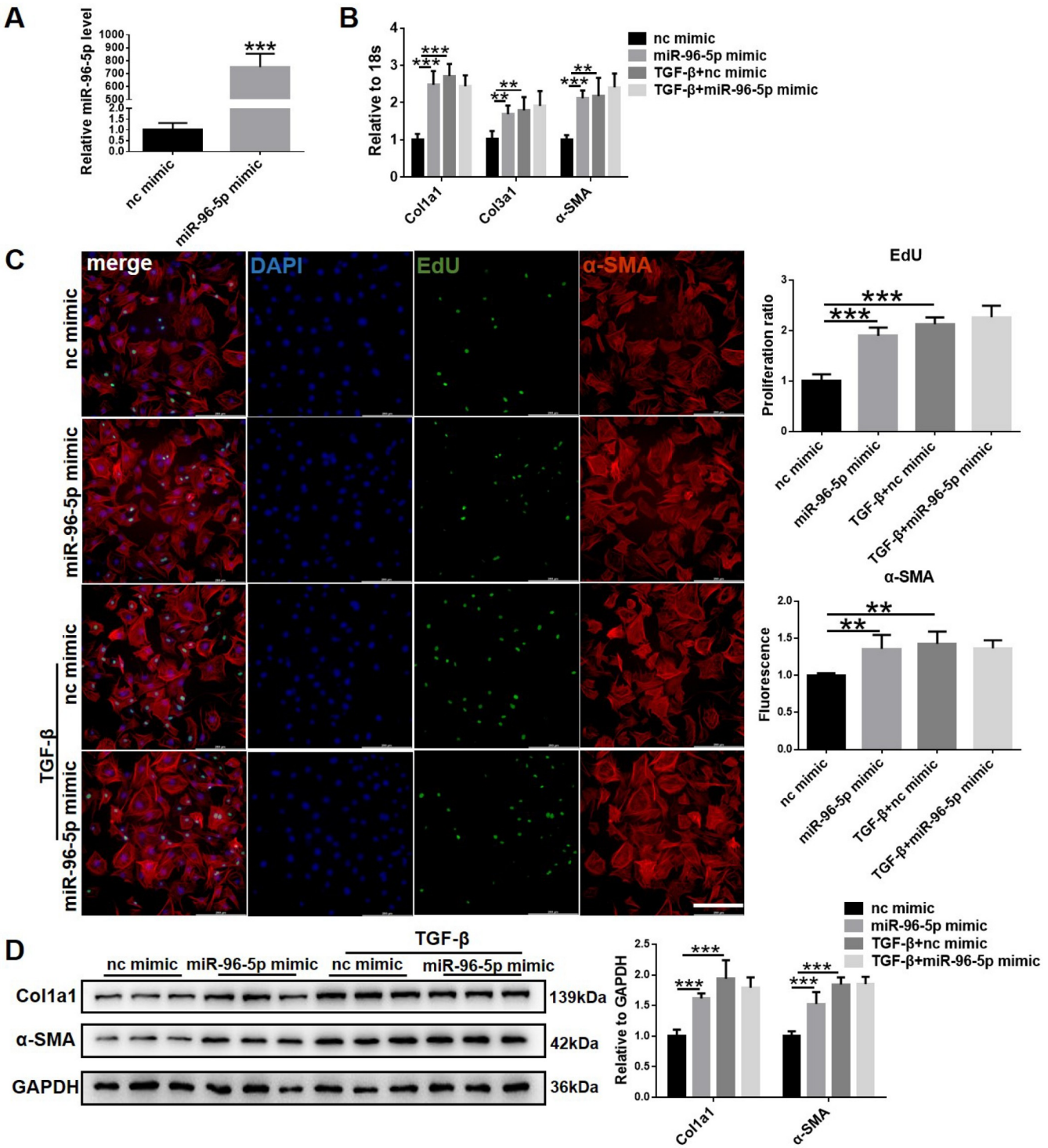

Figure 3. Effect of miR-96-5p mimic on the fibrosis degree of NRCFs stimulated by TGF-β (A) Expression of miR-96-5p in NRCFs transfected with mimic ($n=5$). (B) Relative mRNA levels of fibrosis-associated genes normalized to 18 s in NRCFs ($n=5$). (C) NRCF proliferation was evaluated using EdU, and NRCF differentiation was evaluated using immunofluorescence staining of α-SMA ($n=5$). Scale bar: 200 μm. (D) Western blot analysis was performed to determine the protein levels of Col1a1 and α-SMA in NRCFs ($n=6$). $^{**}P<0.01$, $^{***}P<0.001$ vs corresponding controls.

assay and functional rescue experiment revealed that miR-96-5p promoted cardiac fibrosis by directly targeting the downstream Smad7/Smad3 signaling pathway.

The number of MI patients and relevant medical insurance costs have been rising annually, and optimal therapies are urgently needed for MI [36]. Most chronic cardiovascular diseases are characterized by pathological features of cardiac fibrosis [16]. Control of fibrosis is beneficial in attenuating heart failure caused by

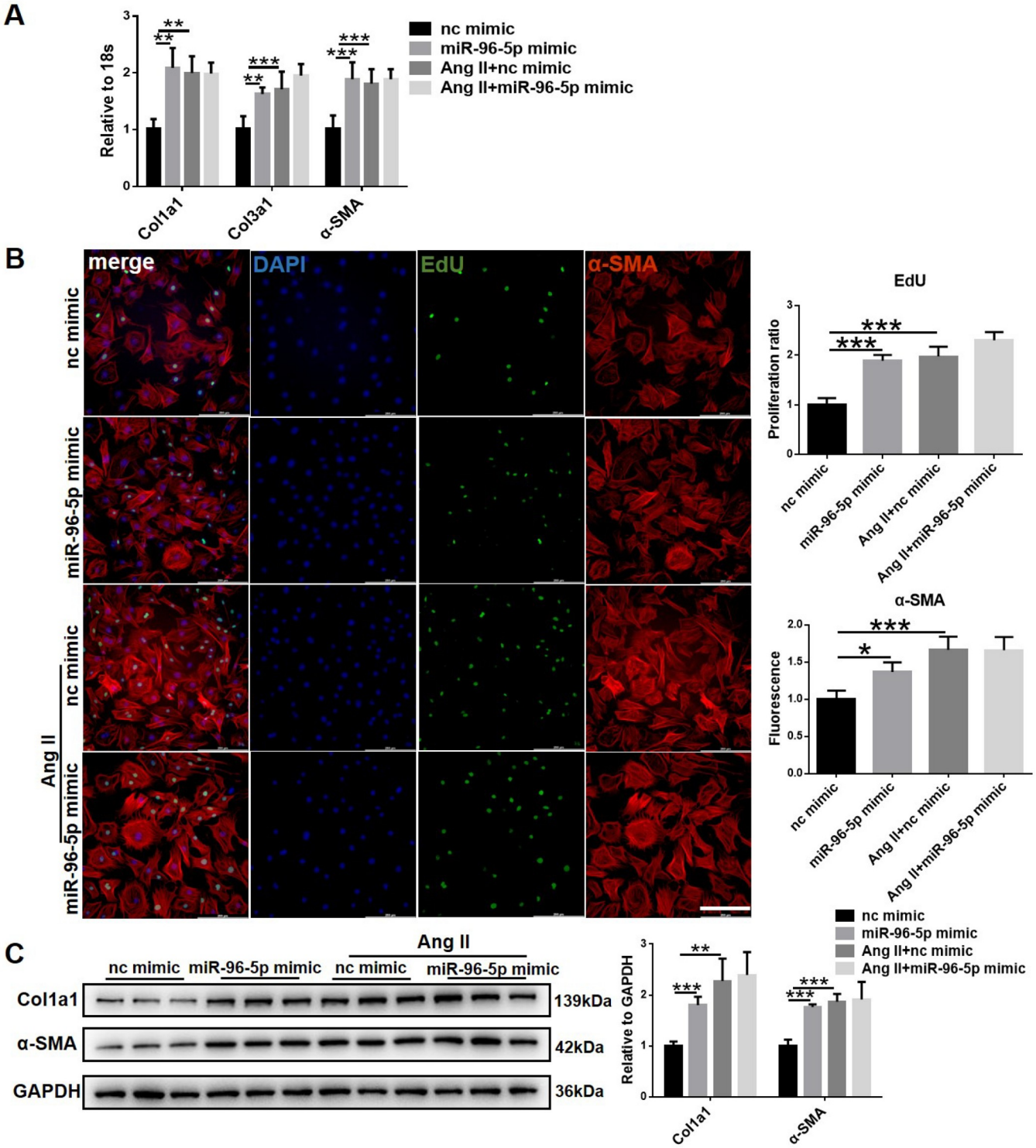

Figure 4. Effect of miR-96-5p mimic on NRCFs in the presence of Ang II (A) qPCR was used to detect the mRNA levels of profibrotic genes in NRCFs ($n=5$). (B) Proliferation and differentiation of NRCFs determined by immunofluorescence staining of EdU and α-SMA ($n=5$). Scale bar: 200 μm. (C) Protein expressions of Col1a1 and α-SMA in NRCFs ($n=6$). $^*P<0.05$, $^{**}P<0.01$, $^{***}P<0.001$ vs corresponding controls.

myocardial infarction. Unfortunately, a cure for cardiac fibrosis has not yet been developed [37]. Various studies have focused on the roles of miRNAs in different types of human disorders, including cardiac fibrosis. Manipulation of these miRNAs seems to be a promising therapeutic modality for fibrosis [38].

Previous research concerning the roles of miR-96-5p in tumors and fibrosis reached contradictory conclusions. miR-96-5p was found to enhance the proliferative and migratory abilities of breast

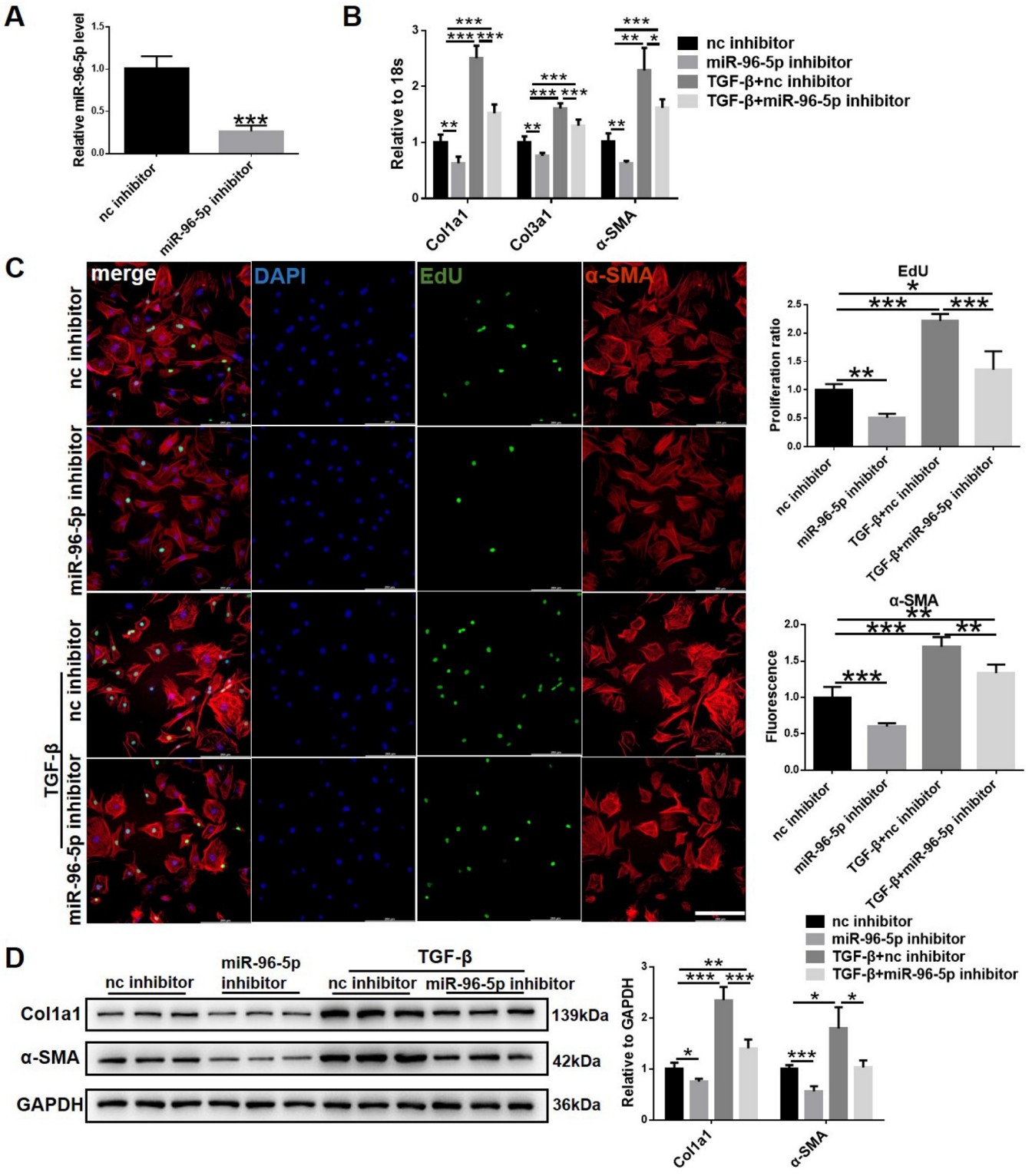

Figure 5. miR-96-5p inhibition suppresses the level of fibrosis in NRCFs in the presence of TGF-β (A) Expression of miR-96-5p in NRCFs transfected with inhibitor ($n=5$). (B) Relative mRNA levels of Col1a1, Col3a1, and α-SMA normalized to 18 s in NRCFs ($n=5$). (C) Proliferation and differentiation degree of NRCFs evaluated by EdU/α-SMA staining ($n=5$). Scale bar: 200 μm. (D) Western blot analysis of the protein levels of fibrosis-related genes in NRCFs ($n=6$). $^{*}P<0.05$, $^{**}P<0.01$, $^{***}P<0.001$ vs corresponding controls.

cancer cells [39]. In contrast, it inhibited the proliferation of pancreatic carcinoma cells [40]. For liver and renal fibrosis, miR-96-5p suppressed profibrogenic activation of hepatic stellate cells [22] and restrained fibrosis in diabetic kidney disease [23]. These studies

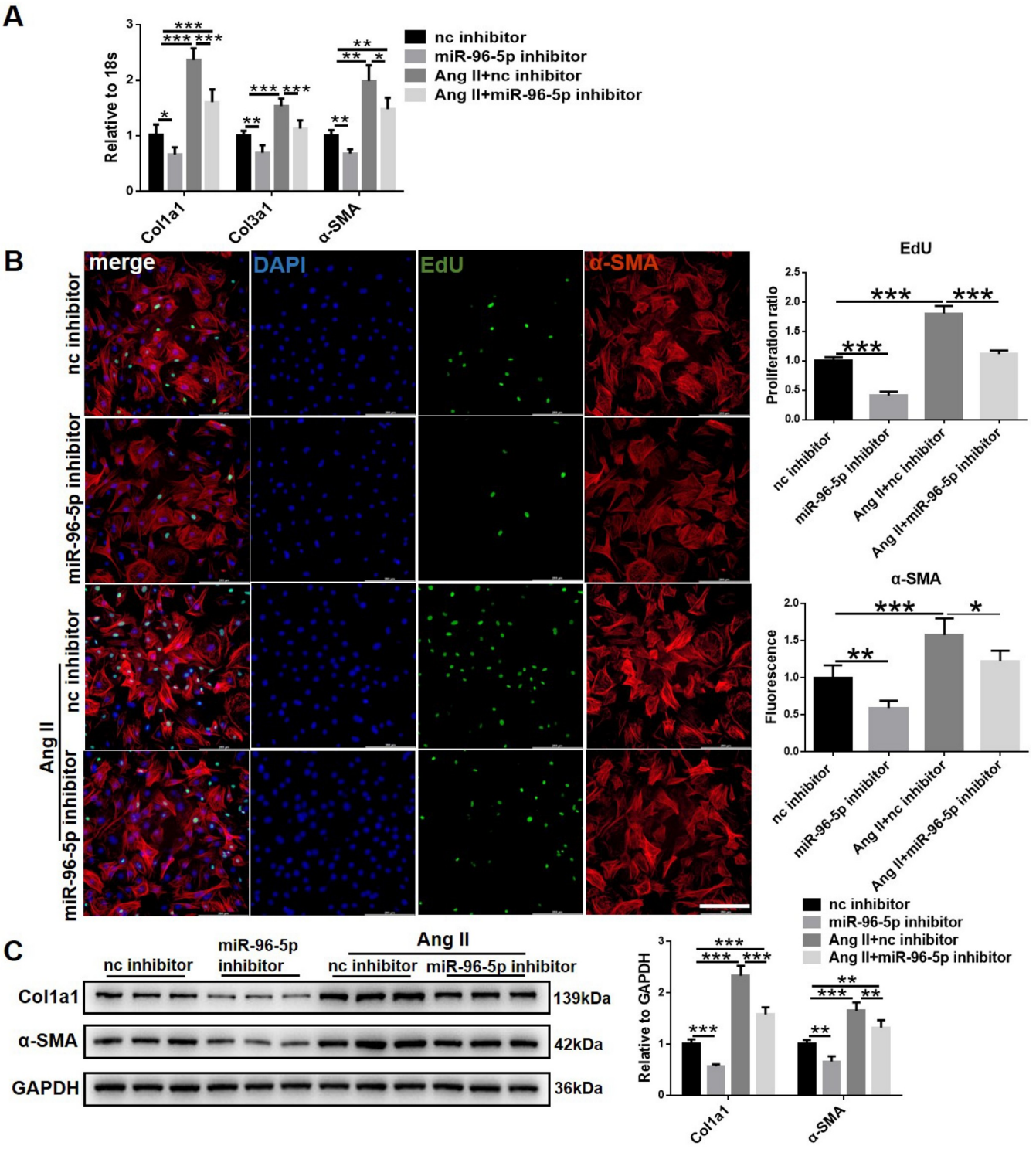

Figure 6. miR-96-5p inhibitor impedes the proliferation and differentiation abilities of NRCFs treated with Ang II (A) Relative mRNA levels of Col1a1, Col3a1, and α-SMA detected by qPCR ($n=5$). (B) NRCF proliferation was indicated by EdU staining, while NRCF differentiation was indicated by α-SMA staining ($n=5$). Scale bar: 200 μm. (C) Protein levels of fibrosis-associated genes in NRCFs detected by western blot analysis ($n=6$). $^{*}P<0.05$, $^{**}P<0.01$, $^{***}P<0.001$ vs corresponding controls.

imply that miR-96-5p has an intricate cell- or tissue-based specific effect on fibrosis and cancer. Nevertheless, its role in cardiac fibrosis has not yet been elucidated.

miR-96-5p was selected as a potential cardiac fibrosis-associated microRNA from the miR-seq in view of its upregulation in cardiac tissues post-MI. It was consistently increased in the two fibrotic cell

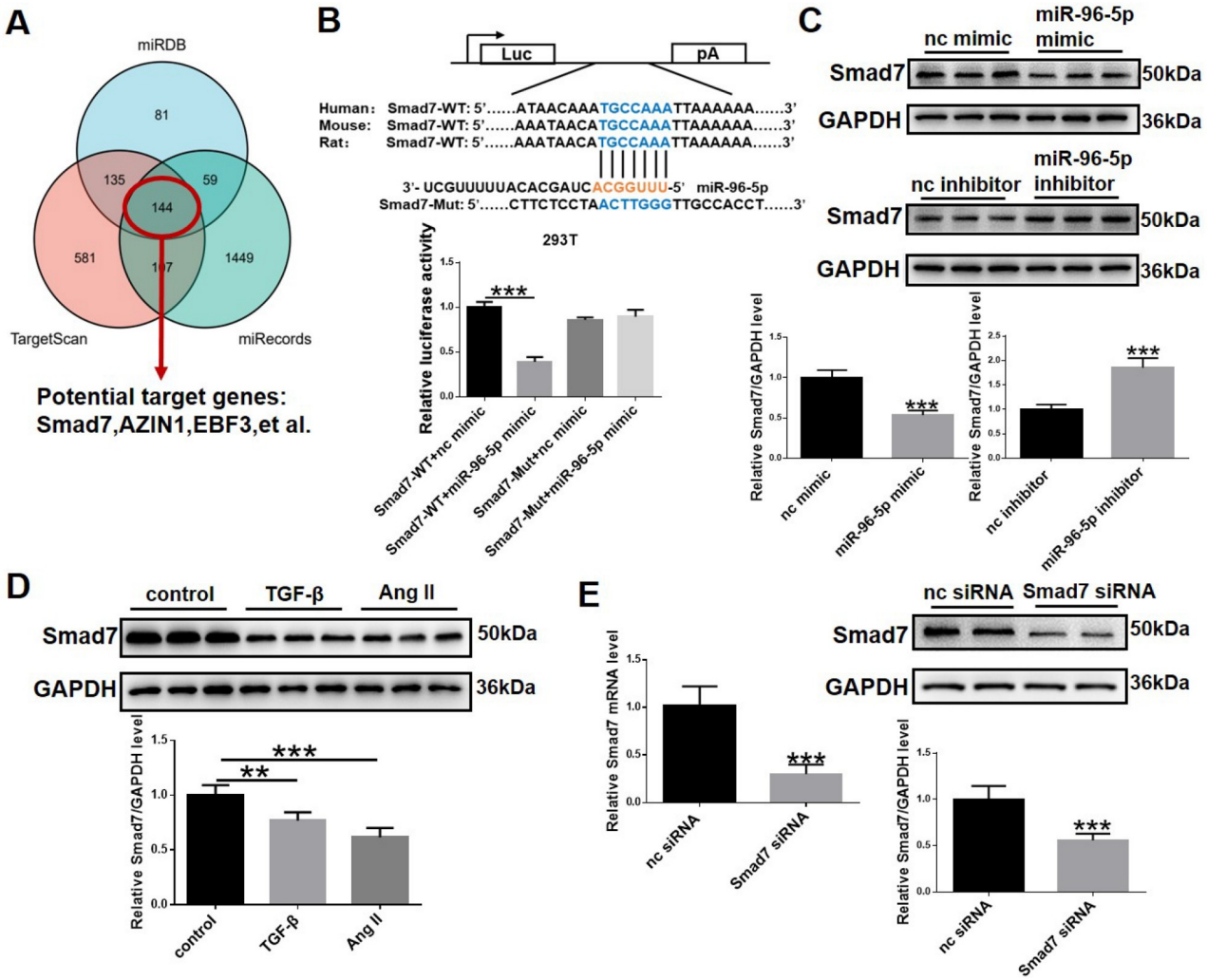

Figure 7. *Smad7* is a direct target of miR-96-5p (A) Potential targets of miR-96-5p were predicted using three databases. (B) *Smad7* was identified as the direct target of miR-96-5p by dual luciferase reporter assay ($n=3$). (C) Protein level of Smad7 in NRCFs treated with miR-96-5p mimic or inhibitor ($n=6$). (D) Protein level of Smad7 in NRCFs stimulated with TGF-β or Ang II ($n=6$). (E) The silencing efficiency of Smad7 siRNA was tested by qPCR and western blot analysis ($n=5$). $^{**}P<0.01$, $^{***}P<0.001$ vs corresponding controls.

models of NRCFs treated with TGF-β or Ang II. This observation is not in line with another study describing that miR-96-5p expression was markedly lower in the serum of acute myocardial infarction patients and H9C2 cells under hypoxic conditions [24]. The animal model employed in our study is a chronic myocardial infarction model. All indicators of the *in vivo* experiments were measured three weeks after MI surgery. Notably, the mechanism underlying the occurrence and progression of fibrosis is complex, and effectors are dynamically regulated in different time periods. However, the *in vivo* experiments merely explored the role of miR-96-5p during the late phase of myocardial fibrosis. Therefore, studies on the acute and subacute phases are warranted to elucidate the optimal time point for manipulating miR-96-5p.

In the case of sham surgery, miR-96-5p expression was significantly downregulated by antagomir, but there was no significant difference in the degree of fibrosis compared to the NC antagomir group. In contrast, miR-96-5p inhibition downregulated the degree of fibrosis at the basal level in the NRCF experiments. This may be attributed to the influence of miR-96-5p on cardiac fibroblasts being simpler *in vitro*, whereas the situation *in vivo* is much more convoluted. Multiple pathways and factors participate in the progression of myocardial fibrosis, and the organism can produce physiological compensation for alterations in miR-96-5p expression. In cellular experiments, the degree of fibrosis was enhanced by the miR-96-5p mimic, whereas the mimic failed to consistently increase the fibrosis level in response to TGF-β or Ang II stimulation, most likely because the additional stimuli caused the cells to approach the upper limit of fibrosis.

The TGF-β1 signaling pathway plays a dominant role in cardiac fibrosis. Current overwhelming evidence shows that the activation of Smad3 is essential for the occurrence and development of cardiac fibrosis [41]. Smad7 can inhibit cardiac fibrosis by blocking Smad3 phosphorylation [29]. Our study established that Smad7 is a cardiac fibrosis-associated downstream effector of miR-96-5p and may mediate its effects through Smad3. Nevertheless, we only studied the underlying mechanism at the cellular level, and it is imperative

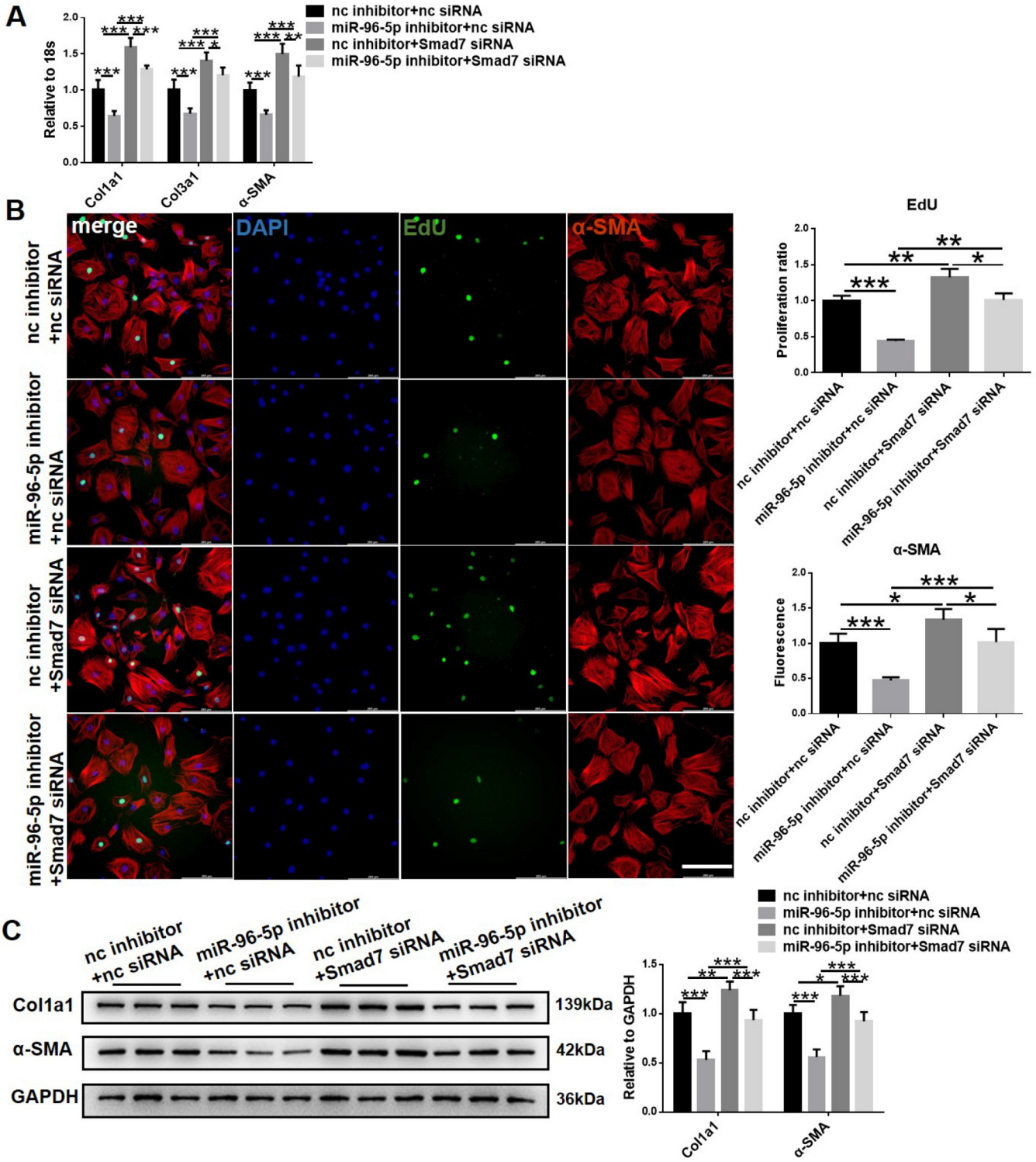

Figure 8. ***Smad7*** **knockdown attenuates the anti-fibrotic effect of the miR-96-5p inhibitor on NRCF** (A) mRNA levels of fibrosis-related genes in NRCFs detected by qPCR ($n=5$). (B) The proliferation and differentiation abilities of NRCFs were assessed by EdU/α-SMA staining ($n=5$). Scale bar: 200 μm. (C) Protein levels of Col1a1 and α-SMA in NRCFs ($n=6$). $^{*}P<0.05$, $^{**}P<0.01$, $^{***}P<0.001$ vs corresponding controls.

to study the phenotype and mechanism in transgenic or knockout mice to validate our results in the future. In addition, blood samples and cardiac biopsy specimens from MI patients will be collected to confirm our results.

In summary, our study identified the biological role of miR-96-5p in promoting cardiac fibrosis by targeting Smad7/Smad3 signaling.

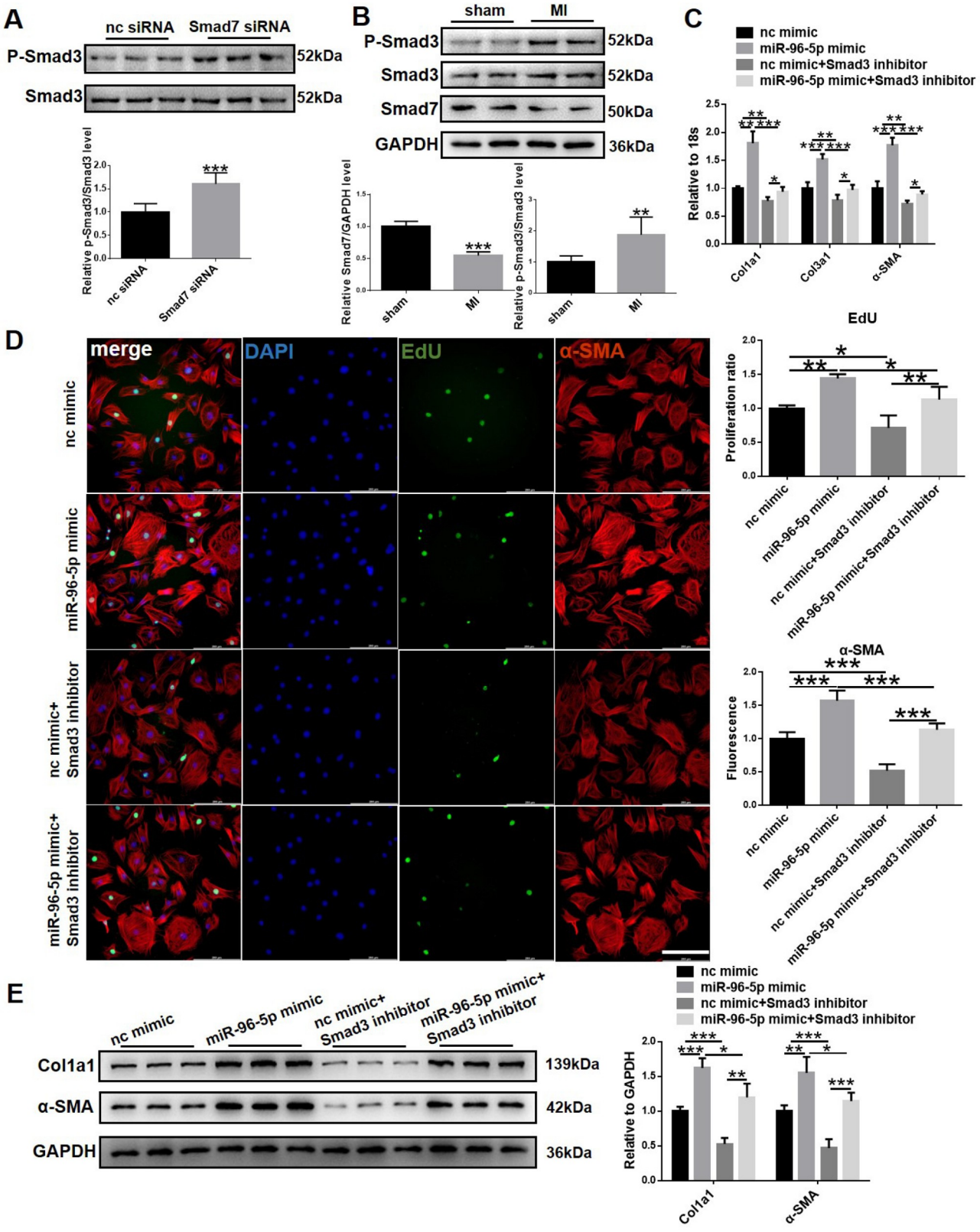

Figure 9. Smad7 mediates the effect of miR-96-5p by enhancing Smad3 phosphorylation (A) Knockdown of *Smad7* activated Smad3 phosphorylation ($n=6$). (B) Protein levels of p-Smad3 and Smad7 in ventricular tissues of sham and MI mice ($n=5$). (C—E) The Smad3 inhibitor weakened the effect of the miR-96-5p mimic on NRCFs, as evidenced by qPCR ($n=5$), EdU/α-SMA staining ($n=5$), and western blot analysis ($n=6$). $^{*}P<0.05$, $^{**}P<0.01$, $^{***}P<0.001$ vs corresponding controls.

This finding provides novel insights into potential therapeutic candidates for fibrosis post MI.

Supplementary Data

Supplementary data is available at *Acta Biochimica et Biphysica Sinica* online.

Funding

This work was supported by the grants from the National Natural Science Foundation of China (No. 81900220) and the Nanjing Health Bureau Medical Science and Technology Development Foundation (No. YKK19052).

Conflict of Interest

The authors declare that they have no conflict of interest.

References

1. Adams E, McCloy R, Jordan A, Falconer K, Dykes IM. Direct reprogramming of cardiac fibroblasts to repair the injured Heart. *J Cardiovasc Dev Dis* 2021, 8: 72
2. Mia MM, Cibi DM, Ghani SABA, Singh A, Tee N, Sivakumar V, Bogireddi H, *et al.* Loss of Yap/Taz in cardiac fibroblasts attenuates adverse remodelling and improves cardiac function. *Cardiovasc Res* 2022, 118: 1785–1804
3. Gan W, Ren J, Li T, Lv S, Li C, Liu Z, Yang M. The SGK1 inhibitor EMD638683, prevents angiotensin II–induced cardiac inflammation and fibrosis by blocking NLRP3 inflammasome activation. *Biochim Biophys Acta Mol Basis Dis* 2018, 1864: 1–10
4. Talman V, Ruskoaho H. Cardiac fibrosis in myocardial infarction—from repair and remodeling to regeneration. *Cell Tissue Res* 2016, 365: 563–581
5. Park S, Nguyen NB, Pezhouman A, Ardehali R. Cardiac fibrosis: potential therapeutic targets. *Transl Res* 2019, 209: 121–137
6. Liang J, Zou X, Fang X, Xu J, Xiao Z, Zhu J, Li H, *et al.* The Smad3-miR-29b/miR-29c axis mediates the protective effect of macrophage migration inhibitory factor against cardiac fibrosis. *Biochim Biophys Acta Mol Basis Dis* 2019, 1865: 2441–2450
7. Zhao H, Yang H, Geng C, Chen Y, Tang Y, Li Z, Pang J, *et al.* Elevated IgE promotes cardiac fibrosis by suppressing miR-486a-5p. *Theranostics* 2021, 11: 7600–7615
8. Khalil H, Kanisicak O, Vagnozzi RJ, Johansen AK, Maliken BD, Prasad V, Boyer JG, *et al.* Cell-specific ablation of Hsp47 defines the collagen-producing cells in the injured heart. *JCI Insight* 2019, 4: e128722
9. Leask A. Potential therapeutic targets for cardiac fibrosis. *Circ Res* 2010, 106: 1675–1680
10. Blyszczuk P, Müller-Edenborn B, Valenta T, Osto E, Stellato M, Behnke S, Glatz K, *et al.* Transforming growth factor-β-dependent Wnt secretion controls myofibroblast formation and myocardial fibrosis progression in experimental autoimmune myocarditis. *Eur Heart J* 2016, 38: 1413
11. Larson C, Oronsky B, Carter CA, Oronsky A, Knox SJ, Sher D, Reid TR. TGF-beta: a master immune regulator. *Expert Opin Therapeutic Targets* 2020, 24: 427–438
12. Bartel DP. MicroRNAs: target recognition and regulatory functions. *Cell* 2009, 136: 215–233
13. Piccoli MT, Gupta SK, Thum T. Noncoding RNAs as regulators of cardiomyocyte proliferation and death. *J Mol Cell Cardiol* 2015, 89: 59–67
14. Deng HY, He ZY, Dong ZC, Zhang YL, Han X, Li HH. MicroRNA-451a attenuates angiotensin II–induced cardiac fibrosis and inflammation by directly targeting T-box1. *J Physiol Biochem* 2022, 78: 257–269
15. Gupta SK, Itagaki R, Zheng X, Batkai S, Thum S, Ahmad F, Van Aelst LN, *et al.* miR-21 promotes fibrosis in an acute cardiac allograft transplantation model. *Cardiovasc Res* 2016, 110: 215–226
16. Yang K, Shi J, Hu Z, Hu X. The deficiency of miR-214-3p exacerbates cardiac fibrosis via miR-214-3p/NLRC5 axis. *Clin Sci* 2019, 133: 1845–1856
17. Yu Y, Zhang Y, Ding Y, Bi X, Yuan J, Zhou H, Wang P, *et al.* MicroRNA-99b-3p promotes angiotensin II-induced cardiac fibrosis in mice by targeting GSK-3β. *Acta Pharmacol Sin* 2021, 42: 715–725
18. Dong Q, Long X, Cheng J, Wang W, Tian Q, Di W. LncRNA GAS5 suppresses ovarian cancer progression by targeting the miR-96-5p/PTEN axis. *Ann Transl Med* 2021, 9: 1770
19. Liu Z, Cui Y, Wang S, Wu C, Mei F, Han E, Hu Z, *et al.* MiR-96-5p is an oncogene in lung adenocarcinoma and facilitates tumor progression through ARHGAP6 downregulation. *J Appl Genet* 2021, 62: 631–638
20. Kang J, Li Y, Zou Y, Zhao Z, Jiao L, Zhang H. miR-96-5p induces orbital fibroblasts differentiation by targeting Smad7 and promotes the development of thyroid-associated ophthalmopathy. *Evid Based Complement Alternat Med* 2022, 2022: 8550307
21. Singh AK, Rooge SB, Varshney A, Vasudevan M, Bhardwaj A, Venugopal SK, Trehanpati N, *et al.* Global microRNA expression profiling in the liver biopsies of hepatitis B virus–infected patients suggests specific microRNA signatures for viral persistence and hepatocellular injury. *Hepatology* 2018, 67: 1695–1709
22. Yu K, Li N, Cheng Q, Zheng J, Zhu M, Bao S, Chen M, *et al.* miR-96-5p prevents hepatic stellate cell activation by inhibiting autophagy via ATG7. *J Mol Med* 2018, 96: 65–74
23. Wang W, Jia Y, Yang Y, Xue M, Zheng Z, Wang L, Xue Y. LncRNA GAS5 exacerbates renal tubular epithelial fibrosis by acting as a competing endogenous RNA of miR-96-5p. *Biomed Pharmacother* 2020, 121: 109411
24. Ding H, Chen W, Chen X. Serum miR-96-5p is a novel and non-invasive marker of acute myocardial infarction associated with coronary artery disease. *Bioengineered* 2022, 13: 3930–3943
25. Frangogiannis NG. Transforming growth factor–β in tissue fibrosis. *J Exp Med* 2020, 217
26. Lan HY. Diverse roles of TGF-β/Smads in renal fibrosis and inflammation. *Int J Biol Sci* 2011, 7: 1056–1067
27. Bujak M, Frangogiannis N. The role of TGF-β signaling in myocardial infarction and cardiac remodeling. *Cardiovasc Res* 2007, 74: 184–195
28. Jia L. Angiotensin II induces inflammation leading to cardiac remodeling. *Front Biosci* 2012, 17: 221–231
29. Wei LH, Huang XR, Zhang Y, Li YQ, Chen H, Yan BP, Yu CM, *et al.* Smad7 inhibits angiotensin II-induced hypertensive cardiac remodelling. *Cardiovasc Res* 2013, 99: 665–673
30. Kato M, Putta S, Wang M, Yuan H, Lanting L, Nair I, Gunn A, *et al.* TGF-β activates Akt kinase through a microRNA-dependent amplifying circuit targeting PTEN. *Nat Cell Biol* 2009, 11: 881–889
31. Yuan J, Chen H, Ge D, Xu Y, Xu H, Yang Y, Gu M, *et al.* Mir-21 promotes cardiac fibrosis after myocardial infarction via targeting smad7. *Cell Physiol Biochem* 2017, 42: 2207–2219
32. Livak KJ, Schmittgen TD. Analysis of relative gene expression data using real-time quantitative PCR and the $2^{-\Delta\Delta CT}$ method. *Methods* 2001, 25: 402–408
33. Gao X, Li H, Zhang W, Wang X, Sun H, Cao Y, Zhao Y, *et al.* Photobiomodulation drives MiR-136-5p expression to promote injury repair after myocardial infarction. *Int J Biol Sci* 2022, 18: 2980–2993
34. Zeng N, Huang YQ, Yan YM, Hu ZQ, Zhang Z, Feng JX, Guo JS, *et al.* Diverging targets mediate the pathological role of miR-199a-5p and miR-199a-3p by promoting cardiac hypertrophy and fibrosis. *Mol Ther Nucleic Acids* 2021, 26: 1035–1050
35. Zhang L, Bian Y, Bai R, Song X, Liang B, Xiao C. Circ_BMP2K enhances

the regulatory effects of miR-455-3p on its target gene *SUMO1* and thereby inhibits the activation of cardiac fibroblasts. *Biochem Cell Biol* 2020, 98: 583–590

36. Li C, Chen X, Huang J, Sun Q, Wang L. Clinical impact of circulating miR-26a, miR-191, and miR-208b in plasma of patients with acute myocardial infarction. *Eur J Med Res* 2015, 20: 58
37. Segura AM, Frazier OH, Buja LM. Fibrosis and heart failure. *Heart Fail Rev* 2014, 19: 173–185
38. Nagpal V, Rai R, Place AT, Murphy SB, Verma SK, Ghosh AK, Vaughan DE. MiR-125b is critical for fibroblast-to-myofibroblast transition and cardiac fibrosis. *Circulation* 2016, 133: 291–301
39. Qin W, Feng S, Sun Y, Jiang G. MiR-96-5p promotes breast cancer migration by activating MEK/ERK signaling. *J Gene Med* 2020, 22: e3188
40. Li C, Du X, Tai S, Zhong X, Wang Z, Hu Z, Zhang L, ***et al.*** GPC1 regulated by miR-96-5p, rather than miR-182-5p, in inhibition of pancreatic carcinoma cell proliferation. *Int J Mol Sci* 2014, 15: 6314–6327
41. Dobaczewski M, Bujak M, Li N, Gonzalez-Quesada C, Mendoza LH, Wang XF, Frangogiannis NG. Smad3 signaling critically regulates fibroblast phenotype and function in healing myocardial infarction. *Circ Res* 2010, 107: 418–428